Available online at www.sciencedirect.com
ScienceDirect
Ceramics International 34 (2008) 985–989
CERAMICS INTERNATIONAL
www.elsevier.com/locate/ceramint

Improvement in crystal orientation of AlN thin films prepared on Mo electrodes using AlN interlayers

Toshihiro Kamohara [a,b], Morito Akiyama [a,*], Naohiro Ueno [a], Noriyuki Kuwano [c]

[a] *On-site Sensing and Diagnosis Research Laboratory, National Institute of Advanced Industrial Science and Technology (AIST), Saga 841-0052, Japan*

[b] *Department of Applied Science for Electronics and Materials, Graduate School of Engineering Sciences, Kyushu University, Fukuoka 816-8580, Japan*

[c] *Art, Science and Technology Center for Cooperative Research, Kyushu University, Fukuoka 816-8580, Japan*

Available online 29 September 2007

Abstract

Highly *c*-axis oriented aluminum nitride (AlN) thin films have been prepared on molybdenum (Mo) bottom electrodes using AlN interlayers (AlN-IL), by reactive rf magnetron sputtering. The interlayers were deposited between the Mo electrodes and silicon substrates, such as AlN/Mo/AlN-IL/Si. The crystallinity and crystal orientation of the interlayers depend on the interlayer thickness and strongly influence those of the Mo electrodes and AlN films. From transmission electron microscopy observations and X-ray pole figure measurements, the interlayer, Mo electrode and AlN film consist of columnar grains and exhibit a fiber texture. It has been found that they have the local epitaxial relationship of $(0\,0\,0\,1)\,[2\,\bar{1}\,\bar{1}\,0]$ AlN-IL//$(1\,1\,0)[\bar{1}\,1\,1]$ Mo//$(0\,0\,0\,1)\,[2\,\bar{1}\,\bar{1}\,0]$ AlN. The nucleation process of AlN thin films changes from a fine grain structure to a columnar structure.

Keywords: A. Films; B. Electron microscopy; Crystal orientation; AlN

1. Introduction

The rapid advancement of mobile communications has required high frequency band-pass filters. Film bulk acoustic resonator (FBAR) filters are well suited for mobile communication systems operating at high frequencies in the GHz range. In FBAR filters, the total thickness, electromechanical coupling coefficient and acoustic material quality determine the operating frequency, bandwidth and insertion loss, respectively.

Aluminum nitride (AlN) is one of the most promising candidates as a piezoelectric material for FBAR, because AlN has a high bulk acoustic wave velocity, a high electrical resistance, a wide band gap and compatibility with silicon processing [1]. AlN has a wurtzite crystal structure with *a*-axis of 0.3112 nm and *c*-axis of 0.4982 nm [2]. If highly *c*-axis oriented AlN films are grown, the high electromechanical coupling coefficient and low loss can be achieved. In addition, it is important to select bottom electrode materials in FBAR, because the acoustic waves generated pass through an entire resonating stack. AlN films preferentially grow in the *c*-axis on various metal electrodes, such as (1 1 1) Pt, (1 1 1) Au and (1 1 1) Al electrodes due to the lattice match [3]. However, Pt and Au electrodes are difficult to deposit directly on substrates and to be etched out. Al electrodes also have problems of surface oxidation and etching selectivity with AlN. Molybdenum (Mo) has some superior properties as FBAR electrodes, because it has low acoustic attenuation, high electrical conductivity, high adhesion strength with AlN and good etching capability [4]. Although Mo electrodes have such clear advantages, it is difficult to prepare highly crystal oriented AlN films on Mo bottom electrodes. Recently, a few researchers have successfully prepared highly oriented AlN films on polycrystalline Mo bottom electrodes by optimizing the reactive sputtering conditions [4,5].

In this work, the crystal growth of highly ***c***-axis oriented AlN films on Mo bottom electrodes was investigated using AlN interlayers (AlN-IL) between the electrodes and silicon substrates, such as AlN/Mo/AlN-IL/Si. Furthermore the microstructure of the films was analyzed and the crystal-

* Corresponding author. Tel.: +81 942 81 3665; fax: +81 942 81 3696.
E-mail address: m.akiyama@aist.go.jp (M. Akiyama).

0272-8842/$34.00
doi:10.1016/j.ceramint.2007.09.051

lographic relationship between the AlN and Mo films was revealed.

2. Experimental procedure

AlN interlayers, Mo electrodes and AlN films were prepared on (1 0 0) Si substrates in a rf magnetron sputtering system (CFS-4ES, Tokuda). The distance between the target and substrate was more than 83 mm. The vacuum chamber was evacuated below 2×10^{-4} Pa. The AlN interlayers and AlN films were deposited at 300 °C in 0.5 Pa reactive Ar/N_2 gas mixtures, where the N_2 concentration was 50%. The rf discharge power was 400 W. The target was 3-in. diameter Al (99.999%), and was pre-cleaned at the same deposition condition for 10 min with the shutter closed, before the deposition process commenced. The interlayer thickness altered from 0 to 200 nm, and the thickness of the AlN films was 1 μm. The Mo electrodes were deposited in 0.3 Pa Ar gas and with a power of 100 W. The target was 3-in. diameter Mo (99.9%), and was pre-cleaned at the same deposition condition for 5 min with the shutter closed before the deposition process. The Mo electrode thickness was 200 nm. The crystal structure and crystallinity of the films were examined using X-ray diffraction (XRD: M03X-HF, Mac Science) with Cu Kα radiation. The crystal orientation was evaluated from the full-width at half-maximum (FWHM) of X-ray rocking curves. The in-plane alignment was examined by the X-ray pole figure method (X'Pert-MRD with 4 circle goniometer, Philips). The microstructure was observed by transmission electron microscopy (TEM: JEM-2000EX) operated at 200 kV. TEM samples were prepared with a focused ion beam mill (FB-2000K, Hitachi).

3. Results and discussion

The influence of AlN interlayers on the crystallinity and crystal orientation of AlN films deposited on Mo bottom electrodes was investigated. Fig. 1 shows the XRD patterns of AlN films deposited on (a) Mo/Si and (b) Mo/AlN-IL/Si substrates. Only two peaks due to (0 0 0 2) AlN and (1 1 0) Mo planes were observed in the XRD patterns. Although the deposition conditions of the AlN and Mo were the same, the peak intensities of the AlN film and Mo electrode prepared on the interlayer were 40 times higher than those of the AlN film and Mo electrode directly deposited on the Si substrate. This result indicates that the crystallinity of the AlN film and Mo electrode is significantly improved by the AlN interlayer. The inset of Fig. 1 shows the X-ray rocking curves of the (0 0 0 2) AlN peaks. The FWHM of the rocking curves decreases from 9.1° to 2.5° using the AlN interlayer. This result suggests that the crystal orientation of the AlN film is also improved by the AlN interlayer.

The dependence of the peak intensity of XRD and FWHM of X-ray rocking curves of the AlN interlayers, Mo electrodes and AlN films on the interlayer thickness was investigated in order to clarify the influence of the interlayer thickness on the crystallinity and crystal orientation of the AlN interlayers, Mo electrodes and AlN films. Fig. 2 shows the dependence of the peak intensity of the AlN interlayers, Mo electrodes and AlN

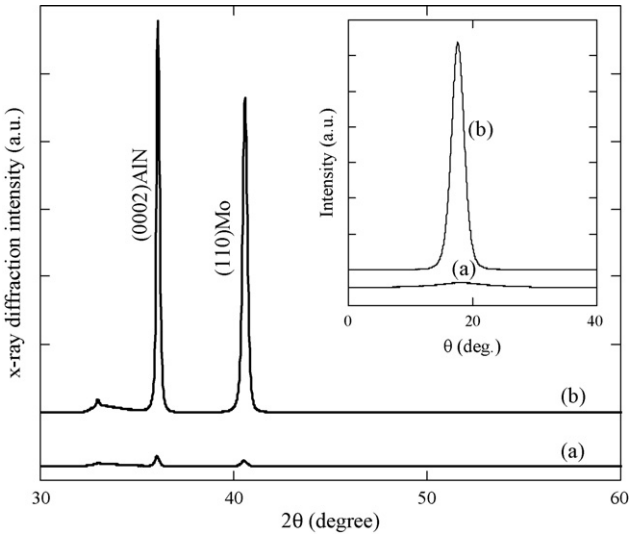

Fig. 1. X-ray diffraction patterns of AlN films prepared on Mo electrodes (a) without an AlN interlayer and (b) with an AlN interlayer. The inset shows the rocking curves of the (0 0 0 2) AlN. The thickness of AlN interlayers, Mo electrodes and AlN films were 200 nm, 200 nm and 1 μm, respectively.

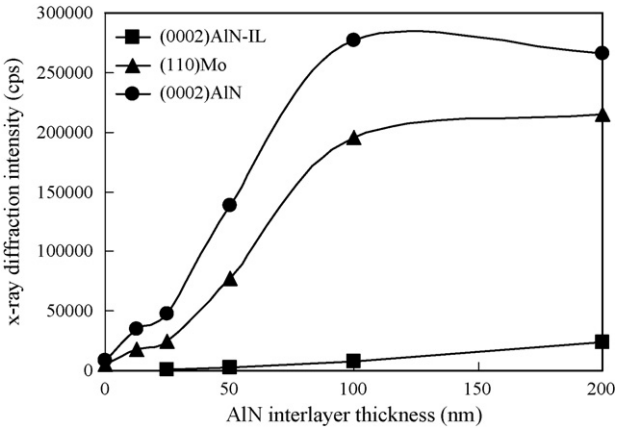

Fig. 2. Dependence of peak intensity of AlN interlayers (■), (1 1 0) Mo electrodes (▲) and (0 0 0 2) AlN films (●) on AlN interlayer thickness.

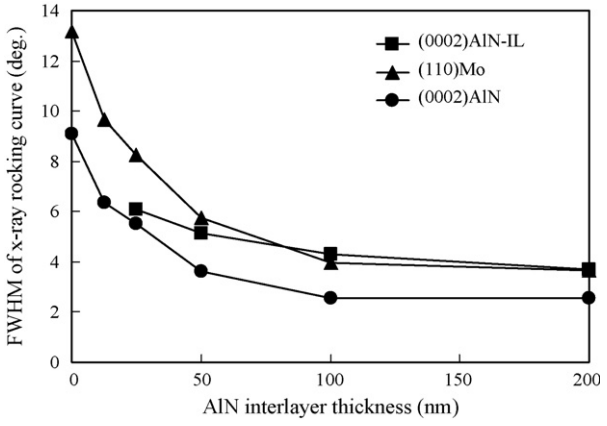

Fig. 3. Dependence of FWHM of X-ray rocking curves reflected from (0 0 0 2) AlN interlayers (■), (1 1 0) Mo electrodes (▲) and (0 0 0 2) AlN films (●) on AlN interlayer thickness.

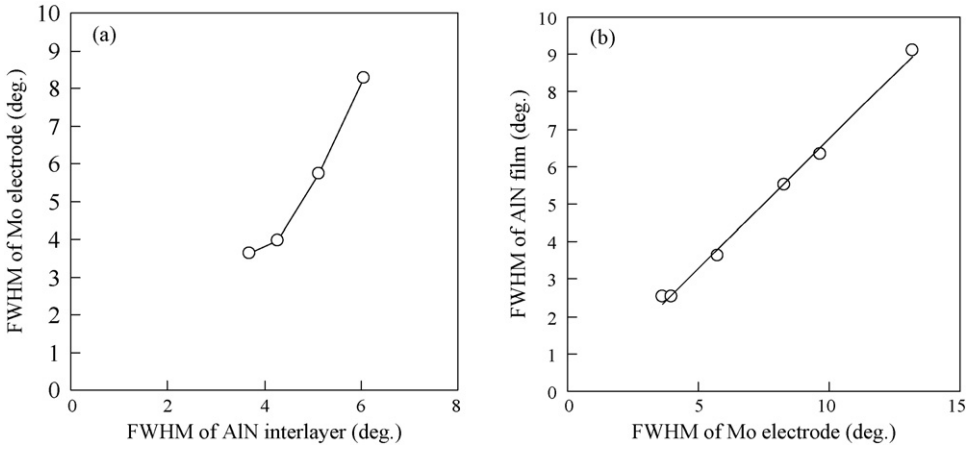

Fig. 4. Relationships of FWHM of X-ray rocking curves (a) between AlN interlayers and Mo electrodes and (b) between Mo electrodes and AlN films.

films on the interlayer thickness. The peak intensity of each layer increases with increasing the interlayer thickness, and the crystallinity of each layer is improved with increasing the interlayer thickness. The peak intensity of the AlN interlayer increases linearly with the thickness. The peak intensities of the Mo and AlN film rapidly increase with increasing interlayer thickness until 100 nm and then saturates. Fig. 3 shows the dependence of the FWHM of X-ray rocking curves of the (0 0 0 2) AlN interlayers, (1 1 0) Mo electrodes and (0 0 0 2) AlN films on the interlayer thickness. The FWHM of each layer decreases with increasing interlayer thickness, and the crystal orientation of each layer is improved with increasing interlayer thickness. The FWHM of the AlN interlayer decreases with increasing thickness. This result is consistent with the reports of

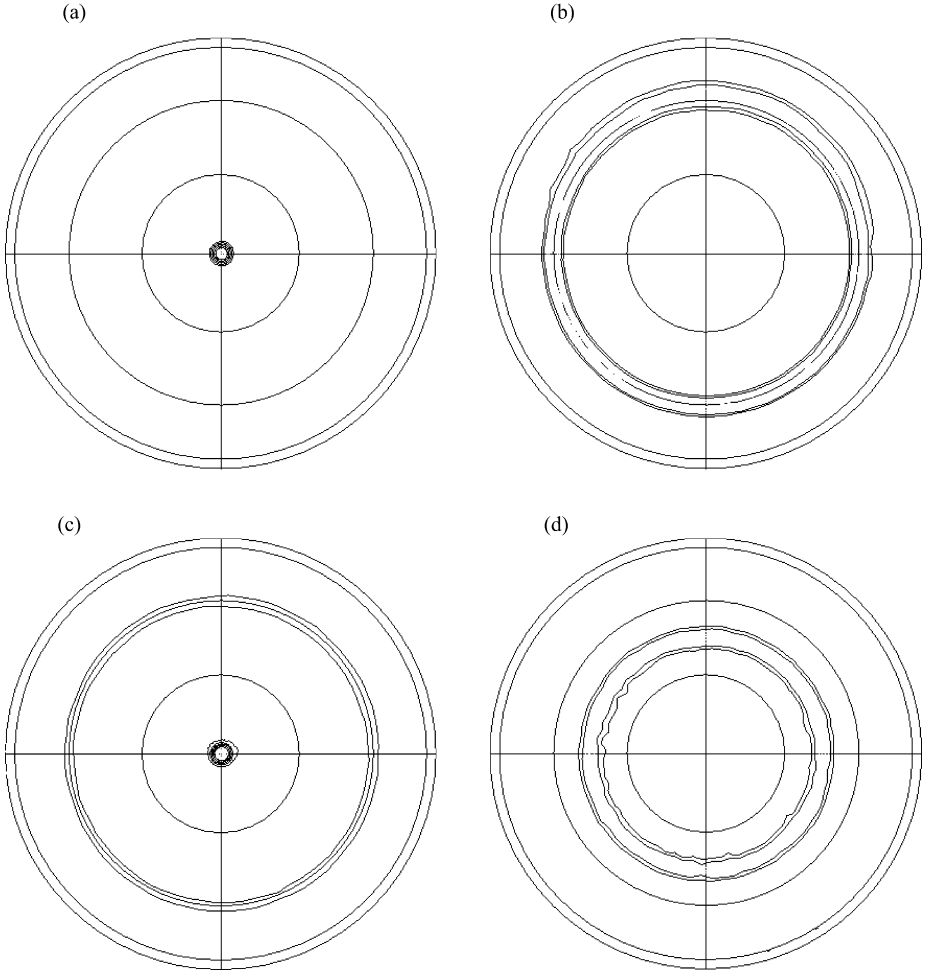

Fig. 5. X-ray pole figures of AlN film and Mo electrode; (a) (0 0 0 2) AlN, (b) $(0\,1\,\bar{1}\,1)$ AlN, (c) (1 1 0) Mo, and (d) (2 0 0) Mo planes.

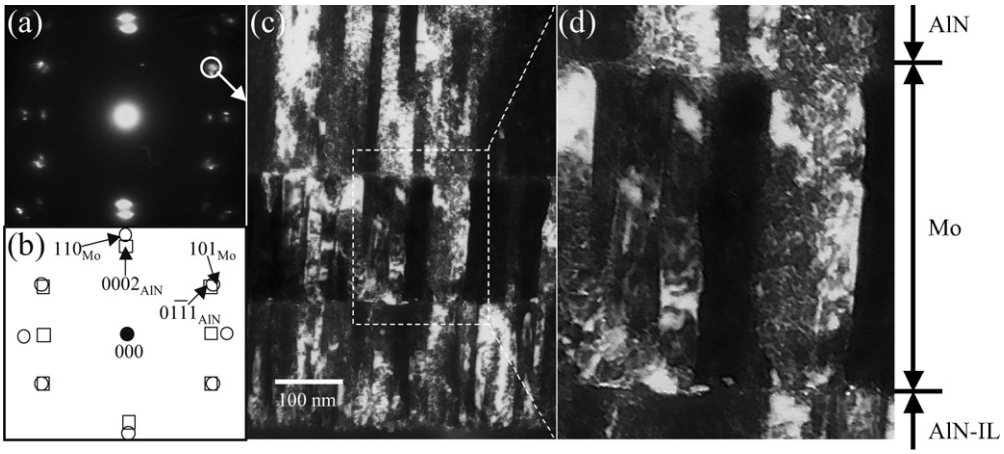

Fig. 6. (a) SAED pattern from mixed region of AlN and Mo, and (b) indexed pattern of (a) (□ and ○ are diffraction spots from AlN and Mo). (c) DF image of AlN/Mo/AlN-IL/Si, taken with the reflection $\boldsymbol{g} = 0\,1\,\bar{1}\,1$ for AlN film and $\boldsymbol{g} = 1\,0\,1$ for Mo film. (d) Localized enlargement of (c).

Hwang et al. [6]. Although the deposition conditions of the Mo electrodes and AlN films are the same, the FWHM of Mo and AlN decreases with increasing interlayer thickness until 100 nm and then saturates. Fig. 4 shows the relationships of the FWHM of X-ray rocking curves (a) between the AlN interlayers and Mo electrodes, and (b) between the Mo electrodes and AlN films. The FWHM of the Mo electrodes increases with increasing the FWHM of the interlayers, and the crystal orientation of the Mo electrodes strongly depends on the crystal orientation of the interlayers, as shown in Fig. 4(a). The FWHM of the AlN films linearly increases with increasing the FWHM of the Mo electrodes, and the crystal orientation of the AlN films strongly depends on the crystal orientation of the Mo electrodes, as shown in Fig. 4(b). Jakkaraju et al. [5] also reported a similar result in that the crystal orientation of AlN films was enhanced with an improvement in the crystal orientation of the bottom electrodes. Thus, it is considered that the AlN interlayers, Mo electrodes and AlN films have strong crystallographic relationships.

Fig. 5 shows the pole figures diffracted from (a) (0 0 0 2) AlN, (b) $(01\bar{1}1)$ AlN, (c) (1 1 0) Mo and (d) (2 0 0) Mo. The central spot in the (0 0 0 2) AlN pole figure and the concentric ring at $\psi = 60^\circ$ in the $(0\,1\,\bar{1}\,1)$ AlN pole figure in Fig. 5(a and b) indicate a strong (0 0 0 1)-fiber texture. The central spot and concentric ring at $\psi = 60^\circ$ in the (1 1 0) Mo pole figure in Fig. 5(c) and concentric ring at $\psi = 45^\circ$ in the (2 0 0) Mo pole figure in Fig. 5(d) suggest a strong (1 1 0)-fiber texture. Fig. 6(a and b) show the selected area electron diffraction (SAED) patterns and the key-diagram taken from an interface between the Mo electrode and the AlN film. The SAED pattern taken from the AlN was composed of two patterns with $[2\,\bar{1}\,\bar{1}\,0]$ and $[0\,1\,\bar{1}\,0]$ incident directions, and the pattern taken from the Mo area was composed of three, with $[\bar{1}\,1\,1]$, [0 0 1] and $[\bar{1}\,1\,0]$ incident directions. These results clearly indicate that the AlN and Mo columns have a (0 0 0 1)-fiber and a (1 1 0)-fiber texture, respectively, which is consistent with the X-ray pole figure results. Fig. 6(c and d) shows dark-field images (DFI) taken with reflections $\boldsymbol{g}$ = 101 for Mo and $\boldsymbol{g} = 0\,1\,\bar{1}\,1$ for AlN in a circle in (a). The diffraction vector $\boldsymbol{g}$ = 1 0 1 for Mo and $\boldsymbol{g} = 0\,1\,\bar{1}\,1$ for AlN are so close to each other, that the DFI taken with the reflection of $\boldsymbol{g}$ = 1 0 1 for Mo also contains a DFI due to $\boldsymbol{g} = 0\,1\,\bar{1}\,1$ for AlN. The AlN interlayer, Mo electrodes and AlN films exhibit a columnar structure ~50 nm in width. Fine crystal nucleation of the AlN is observed at the interface between the substrate and interlayer, and the columnar grains of the AlN and Mo grow on the fine grains, as shown in Fig. 6(c). Therefore, the nucleation process for the AlN thin films changes from a fine grain structures to a columnar structure. Fig. 6(c) clearly shows that the AlN interlayer, Mo electrode and AlN film have a successive columnar structure. The AlN interlayer, Mo electrode and AlN film columnar grains have the heteroepitaxial relationship of $(0\,0\,0\,1)\,[2\,\bar{1}\,\bar{1}\,0]$ AlN-IL// $(1\,1\,0)\,[\bar{1}\,1\,1]$ Mo//$(0\,0\,0\,1)\,[2\,\bar{1}\,\bar{1}\,0]$ AlN, which is comparable to the Burgers relation from bcc to hcp in the martensitic transformation [7,8]. These results clearly indicate that the microstructures of the AlN interlayer, Mo electrode and AlN film are fiber textured and have local heteroepitaxial relationships, as shown in Fig. 7. Some local heteroepitaxial growth in fiber texture was reported [9–11]. However, local heteroepitaxial growth in fiber texture had not been observed in III–V nitride semiconductors. From these results, it could be considered that the crystallinity and orientation of the Mo electrode and AlN film are improved by the AlN interlayer, because the interlayer is effective in decreasing the crystallization energy of the Mo electrode due to the heteroepitaxial nucleation [9].

Furthermore, Zur and McGill reported the criteria for the possibility of heteroepitaxial growth as follows: (1) the area of a

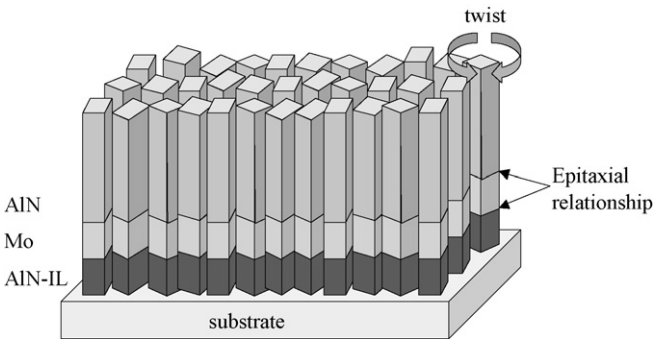

Fig. 7. Schematic illustration of AlN/Mo/AlN-IL structure.

two-dimensional superlattice cell should be less than 600 $Å^2$ and (2) the lattice mismatch at the interface between two-dimensional superlattice cells should be less than 1% [12]. In this study, when the lattice mismatch at the interface between two-dimensional superlattice cells is less than 1%, the area of a two-dimensional superlattice cell is 870 $Å^2$. Therefore, the local heteroepitaxial relationship between an AlN interlayer, Mo electrode and the AlN film, does not satisfy the criteria for heteroepitaxial growth.

4. Conclusions

The crystallinity and crystal orientation of the AlN films prepared on the Mo bottom electrodes are improved by using AlN interlayers. Although the sputtering conditions are the same, the peak intensity of XRD and the FWHM of X-ray rocking curves for the AlN films and Mo bottom electrodes strongly depend on the AlN interlayer thickness. The AlN interlayer, Mo electrode and AlN film exhibit strong (0 0 0 1)- and (1 1 0)-fiber texture. Although the AlN and Mo have different crystal symmetry at the interface, the individual columns of the AlN interlayers, Mo electrodes and AlN films have the local heteroepitaxial relationship of $(0\,0\,0\,1)\,[2\,\bar{1}\,\bar{1}\,0]$ AlN-IL//$(1\,1\,0)\,[\bar{1}\,1\,1]$ Mo//$(0\,0\,0\,1)\,[2\,\bar{1}\,\bar{1}\,0]$ AlN.

References

[1] M.A. Dubois, P. Muralt, Properties of aluminum nitride thin films for piezoelectric transducers and microwave filter applications, Appl. Phys. Lett. 74 (1999) 3032–3034.

[2] S. Strite, H. Morkoc, GaN, AlN, and InN: a review, J. Vac. Sci. Technol. B 10 (1992) 1237–1266.

[3] M.A. Dubois, P. Muralt, Stress and piezoelectric properties of aluminum nitride thin films deposited onto metal electrodes by pulsed direct current reactive sputtering, J. Appl. Phys. 89 (2001) 6389–6395.

[4] S.H. Lee, J.K. Lee, K.H. Yoon, Growth of highly c-axis textured AlN films on Mo electrodes for film bulk acoustic wave resonators, J. Vac. Sci. Technol. A 21 (2003) 1–5.

[5] R. Jakkaraju, G. Henn, C. Shearer, M. Harris, N. Rimmer, P. Rich, Integrated approach to electrode and AlN depositions for bulk acoustic wave (BAW) devices, Microelectron. Eng. 70 (2003) 566–570.

[6] B.H. Hwang, C.S. Chen, H.Y. Lu, T.C. Hsu, Growth mechanism of reactively sputtered aluminum nitride thin films, Mater. Sci. Eng. A 325 (2002) 380–388.

[7] W.G. Burgers, On the process of transition of the cubic-body-centered modification into the hexagonal-close-packed modification of zirconium, Physica 1 (1934) 561–586.

[8] K.J. Caspersen, A. Lew, M. Ortiz, E.A. Carter, Importance of shear in the bcc-to-hcp transformation in iron, Phys. Rev. Lett. 93 (2004) 115501-1–115501-4.

[9] N. Nukaga, M. Mitsuya, T. Suzuki, Y. Nishi, M. Fujimoto, H. Funakubo, Local epitaxial growth of (1 0 3) one-axis-oriented $SrBi_2Ta_2O_9$ thin films prepared at low deposition temperature by metalorganic chemical vapor deposition and their electrical properties, Jpn. J. Appl. Phys. 40 (2001) 5595–5598.

[10] G. Asayama, J. Lettieri, M.A. Zurbuchen, Y. Jia, S. Trolier-McKinstry, D.G. Schlom, S.K. Streiffer, J.-P. Maria, S.D. Bu, C.B. Eom, Growth of (1 0 3) fiber-textured $SrBi_2Nb_2O_9$ films on Pt-coated silicon, Appl. Phys. Lett. 80 (2002) 2371–2373.

[11] H. Kim, C.O. Chui, K.C. Saraswat, P.C. Mclntyre, Local epitaxial growth of ZrO_2 on Ge (1 0 0) substrates by atomic layer epitaxy, Appl. Phys. Lett. 83 (2003) 2647–2649.

[12] A. Zur, T.C. McGill, Lattice match: an application to heteroepitaxy, J. Appl. Phys. 55 (1984) 378–386.